



Open Archive Toulouse Archive Ouverte

OATAO is an open access repository that collects the work of Toulouse researchers and makes it freely available over the web where possible

This is an author's version published in: <https://oatao.univ-toulouse.fr/26631>

Official URL:

<https://doi.org/10.1080/13640461.2020.1778151>

To cite this version:

Freulon, Alexandre  and Trinh, Anh Truc and Lacaze, Jacques  and Malard, Benoît  and Vu, Ke Oanh *Effect of cast iron microstructure on adherence of an epoxy protection*. (2020) International Journal of Cast Metals Research, The. 165-170. ISSN 1364-0461.

Any correspondence concerning this service should be sent to the repository administrator: tech-oatao@listes-diff.inp-toulouse.fr

Effect of cast iron microstructure on adherence of an epoxy protection

Alexandre Freulon^a, Anh Truc Trinh^b, Jacques Lacaze^a, Benoit Malard^a and Ke Oanh Vu^b

^aCIRIMAT, Université de Toulouse, Toulouse, France; ^bInstitute for Tropical Technology, Vietnam Academy of Science and Technology, Hanoi, Vietnam

ABSTRACT

To study the influence of the microstructure of cast iron on the adhesion of an epoxy coating, ferritic, pearlitic and austempered samples were prepared in as-received, polished and oxidised states. A pull-off test (dry adhesion) was performed before immersing in water while the cross-cut test was made after 24 days of exposition in distilled water (wet adhesion). X-rays were combined with optical microscopy (LOM) and scanning electron microscopy (SEM) for surface analysis. The adhesion of the epoxy coating on the cast iron surface firstly depends on the roughness of the surface; polished samples showed high adherence by comparison with as-received samples. On the oxidised samples, the surface oxide significantly improves the adhesion of the coating in both dry and wet states for all three sample microstructure. The presence of carbide in the structure was observed to decrease adherence.

KEYWORDS

Spheroidal graphite cast iron; pearlitic; ferritic; ADI; epoxy coating; adhesion

Introduction

Usual unalloyed cast irons have the same corrosion resistance or are more resistant than usual steels in many applications [1]. Amongst the several possible coatings for improving long-lasting corrosion resistance of cast iron components, epoxies appear as highly versatile ones and give a scratch-resistant finish [1]. In most conditions, graphite shape (lamellar vs. nodular) was reported to have little effect on corrosion resistance of cast irons [2]. In recent literature, a few works have been devoted to corrosion experiments in NaCl solutions [3–7] but only one was dealing with polymer protection of cast iron [8]. The present work was thus intended to investigate the possible effect of surface preparation and cast-iron microstructure on adherence of an epoxy protective layer. The investigation used both pull-off and adherence testing.

Materials and experimental details

Experiments were performed on an industrial nodular cast iron that has been processed to give ferritic, pearlitic and austempered grades. The material was received as three plates $2 \cdot 80 \cdot 80 \text{ mm}^3$ of each grade. Three types of surface treatment were studied in this work: 1) as received; 2) polished with SiC papers from 80 to 1200 grades; 3) thermal treated at 600°C for 3 hours.

Micrographs of the material in the as-received state are presented in Figure 1 for the ferritic and pearlitic grades. It is seen that the so-called ferritic alloy contains some pearlite while the pearlitic one shows some ferrite. The heat-treatment at 600°C did not lead to any noticeable change of the microstructure of the ferritic and pearlitic

grades. In the case of the austempered material, the heat treatment led to limited evolution as can be seen in Figure 2 where are compared the microstructures before (a) and after (b) treatment.

Before coating, all surfaces were initially alkaline degreased at 80°C for 15 min and washed with distilled water and then ethanol, and finally properly dried. The selected coating was a solvent-free epoxy resin, i.e. without solvent or water as diluent. The epoxy resin was diglycidylbisphenol-A (Epon 828, from Hexion) with an equivalent weight of about 185–192 g/eq. The hardener was a low viscosity modified cycloaliphatic polyamine (Ancamine 2735, from Air Products and Chemicals) with an equivalent weight per active H of 95 g/eq. The deposition of the epoxy coating was performed on the whole samples and processed so that its final thickness was about 60 μm which was afterwards controlled with a Minitest FN2 600 from Erichsen. The variation in coating thickness from place to place on any of the samples was found to be $\pm 1 \mu\text{m}$.

The obtained coating is characterised by high density and adherence that make it highly suitable as a primer for subsequent protective or finish surface treatments. For checking the quality of the coating, the conventional adhesion pull-off test was first performed on one of the large surfaces of the samples. This was carried out using Positest Automatic Adhesion Tester following ASTM D-4541 standard. Though only one test was performed on each sample in the present study, the standard deviation of individual measurement may be set at 0.3 MPa on the basis of more extended results obtained on steels [9].

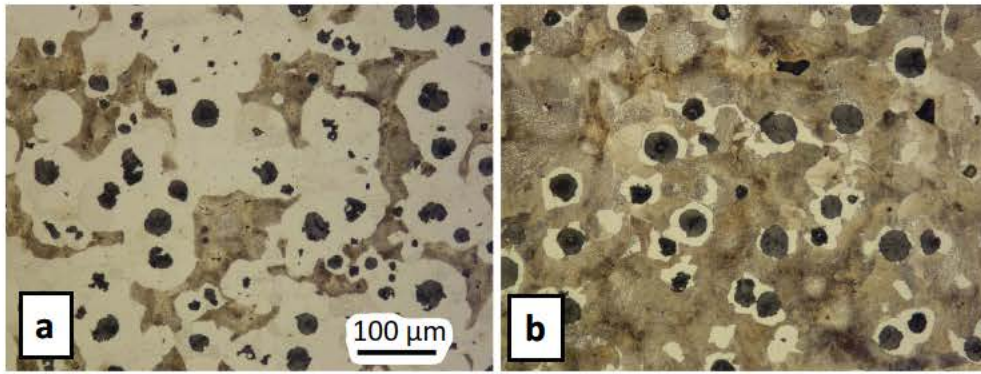


Figure 1. Microstructure after Nital etching of the as-received ferritic (a) and pearlitic (b) materials. The scale is the same for both micrographs.

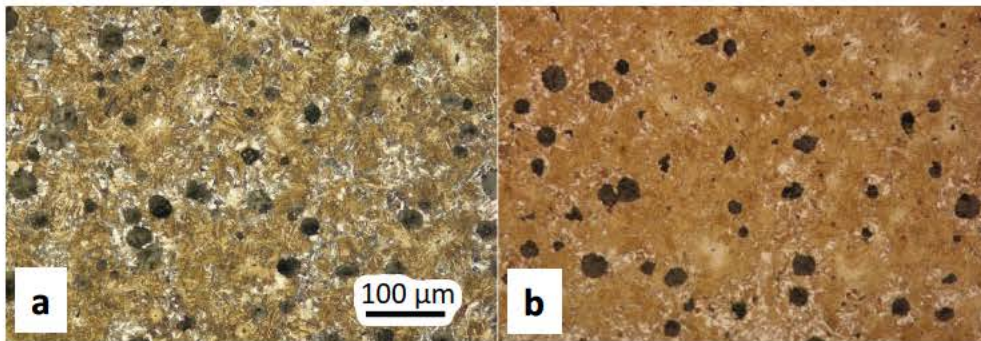


Figure 2. Microstructure after Nital etching of the austempered material, respectively as-received (a) and after heat-treatment (b). The scale is the same for both micrographs.

On the other large surface of each sample, the cross-cut adherence test was performed according to ASTM D-3359 standard (method B) to evaluate the adherence of the coatings after ageing in distilled water. Firstly, cross-hatch cuts with 6 blades spaced by 2 mm between cutting edges were performed. The samples were then immersed in water for 24 days, a duration which appeared necessary by preliminary tests for differentiating the samples. After this exposure, the samples were dried with a clean tissue paper to remove the surface water, and then kept at room temperature for 10 min to be sure of surface dryness. An adhesive tape 50 mm wide with adhesive strength of 9.5 N per 25 mm (ISO 2409) was then applied to the cross-cut coating surface. The tape was removed by a quick pull and the coating removal content was determined. The adhesive strength was evaluated by expressing the adhesive loss as $100 \cdot x / 25$, where x is the number of squares of the coating that have been detached by the tape, with 25 being the total number of squares on the intact coating.

X-rays were performed in conditions allowing getting information from the surface and the substrate. Measurements were carried out with a X-rays beam from a copper anti-cathode (1.5406 Å) which is parallelised by a Gobel mirror. A constant low incidence angle of 10° was set while a Lynxeye XR-T detector was scanned from 10 to 120° .

Small samples were then cut and mounted, and finally prepared for observation by standard metallographic methods. Optical microscopy (LOM) and scanning electron microscopy (SEM) were used to observe the microstructure, the coating and the interface between them.

Results

Pull-off test results in Table 1 showed a very good adherence of the epoxy layer, with effects of the substrate microstructure and of the surface preparation. The pull-off stress was seen to decrease from ferritic to pearlitic, and from pearlitic to austempered matrix structure for all three initial surface states. It should be stressed this applies as well for oxidised samples where it has been seen that the heat-treatment does not significantly modify the matrix structure as compared to the original ausferritized one. X-rays reported later suggest this decrease relates to the increased amount of carbides in the substrate.

Table 1. Pull-off test results (MPa).

| Sample | As-received | Polished | Oxidised |
|-------------|-------------|----------|----------|
| Ferritic | 7.7 | 8.8 | 12.8 |
| Pearlitic | 7.3 | 8.0 | 9.6 |
| Austempered | 6.8 | 7.1 | 8.2 |

For all matrix microstructures, Table 1 showed also that polishing improved adherence and that oxidation did improve it further. It may mean that the surface roughness was too large in the as-received state and that polishing and oxidation did decrease it. The suggested change in surface roughness is illustrated with the micrographs in Figure 3.

After exposure to water during 24 days, adherence results listed in Table 2 showed again a significant effect of surface treatment for the as-received and polished states. It is noteworthy that the as-received material had better properties than the polished one, and also that the ferritic material showed an excellent adherence in both states while the ausferritized one showed deteriorated properties. However, an excellent adherence was obtained for all substrates after pre-oxidation of the material. Though it is generally

Table 2. Adhesive loss (%) after 24 days of exposure in distilled water.

| Sample | As-received | Polished | Oxidised |
|-------------|-------------|----------|----------|
| Ferritic | 0 | 0 | 0 |
| Pearlitic | 0 | 26 | 0 |
| Austempered | 46 | 100 | 0 |

admitted that roughness may improve adhesion [10], it is also known that stresses are generated at surface protrusions which may be decreased with a thin and regular oxide layer.

It appeared of interest to observe more specifically the ferritic samples as all of them are reported as having no loss (Table 2). Figure 4 shows LOM images of the ferritic samples after the adhesive loss test using dark-field conditions to image differently the substrate, the epoxy layer and the mounting. It is seen that only the oxidised sample showed that all of the epoxy

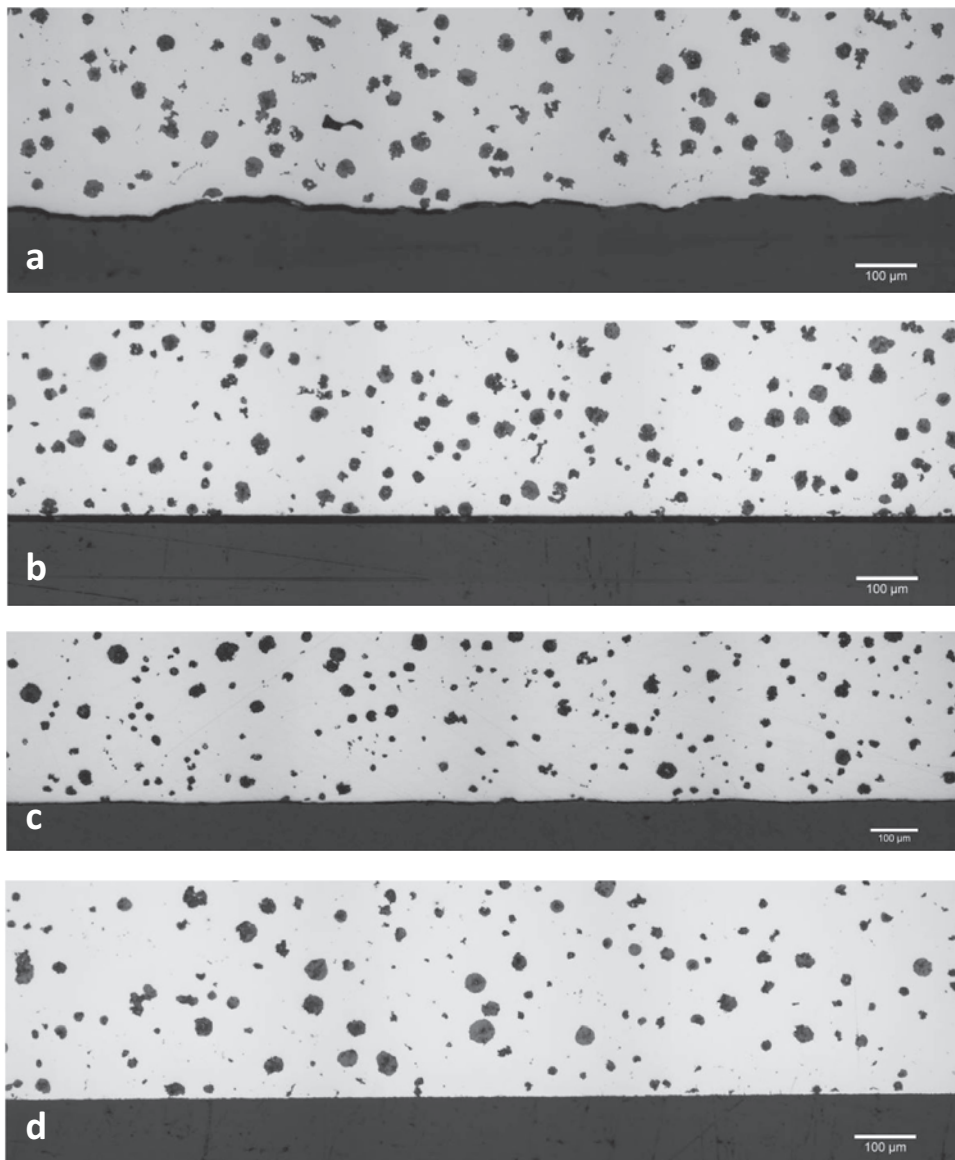


Figure 3. Micrographs showing the surface of ferritic (a and b) and ausferritized (c and d) materials in as received condition (a and c) and after polishing (b and d). The dark area at the bottom of each micrograph is the mounting; the epoxy layer in between the mounting and the material surface can hardly be noticed.

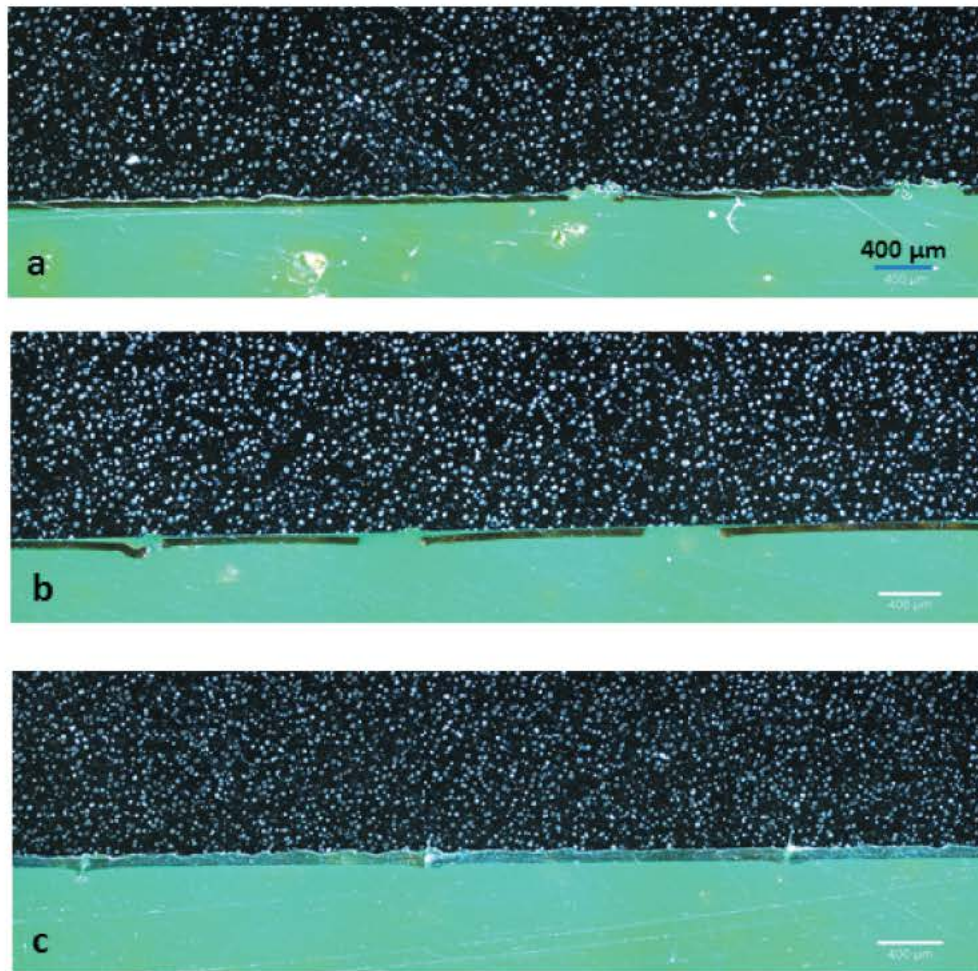


Figure 4. Dark field LOM micrographs of the ferritic samples in the as-received (a) polished (b) and oxidised (c) states. The scale is the same for all three micrographs.

remained effectively attached to the surface. For the other two samples, as-received and polished, the cut area is marked by large gaps in the epoxy layer. In the case of the polished sample (Figure 4(b)), it is seen that these gaps originate from a separation appearing between the epoxy layer and the substrate, which leads or not to a partial breaking-off of the epoxy layer. This improved adherence of the epoxy on the oxidised materials as compared to the other two is in line with results by Wielant [11]. It is thought to relate to the high polarity of epoxy resins which supports the adhesion by favouring the interaction between hydroxyl group or oxirane ring with active hydrogens on the oxide surface.

SEM observations were also performed on all samples which did not allow a clear visualisation of the epoxy layer as no contrast developed between it and the resin used for mounting the samples. As an example, Figure 5 shows a section of the oxidised ferritic alloy where a uniform oxide layer appears at the surface of the substrate. It is clear that this oxide layer has smoothed the small surface irregularities.

X-rays were acquired on all nine samples which are illustrated in Figure 6 with the records acquired on the three oxidised samples. Diffusion due to the polymer is clearly observed for angles in between 10° and 60° . For easing the analysis, this contribution was withdrawn giving records as illustrated in Figure 7 for the same samples.

Table 3 lists the phases observed for all samples using PDF-2 database [12]. The phases corresponding to the cast iron matrix that have been detected are ferrite F (cubic, $a = 2.86 \text{ \AA}$), cementite C (orthorhombic, $a = 5.08 \text{ \AA}$, $b = 6.76 \text{ \AA}$, $c = 4.52 \text{ \AA}$), austenite A (cubic, $a = 3.62 \text{ \AA}$) and Hägg's carbide H (monoclinic, $a = 11.56 \text{ \AA}$, $b = 4.56 \text{ \AA}$, $c = 5.03 \text{ \AA}$). Note that graphite was not detected as very few nodules are expected to be cut by the metallographic section. Hägg's carbide has been sometimes reported in the literature [13,14], it appears when high carbon austenite formed during the first stage of austempering starts decomposing. It is noted in Table 3 that polishing of the austempered sample allowed the low fractions of austenite and Hägg carbide to be detected when they were not with the as-received sample.

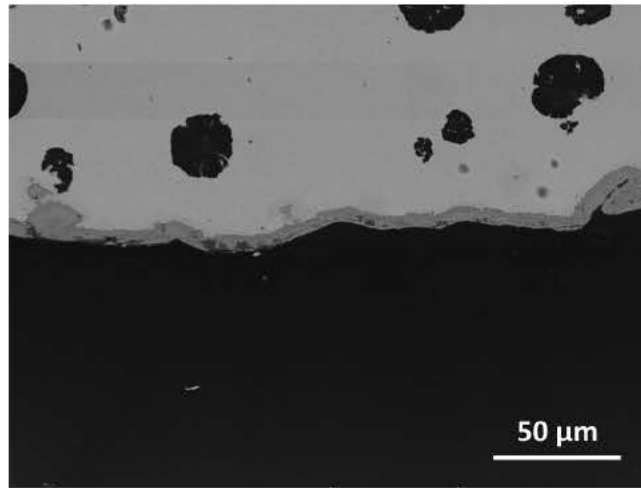


Figure 5. SEM micrograph of the oxidised ferritic alloy.

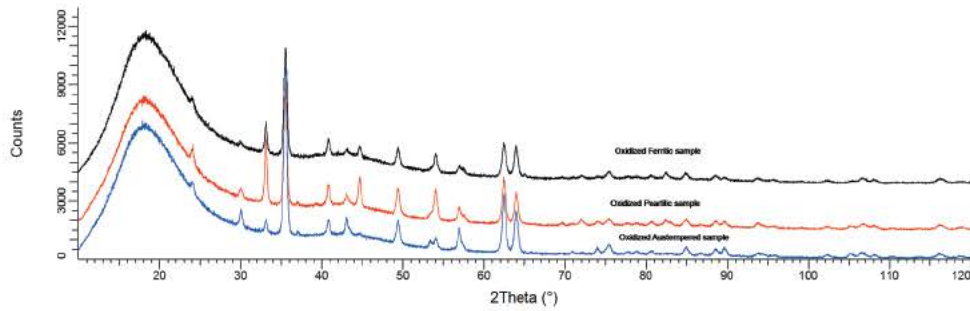


Figure 6. X-ray records for the three oxidised samples. The records have been arbitrarily shifted along the Y axis for clarity.

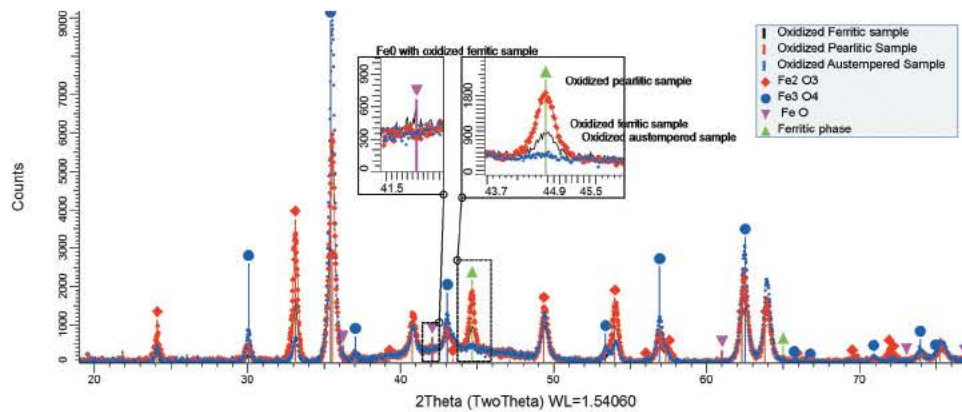


Figure 7. X-ray records for the three oxidised samples after withdrawing of the background due to diffusion of the polymer layer. The insert to the right shows an enlargement of the peak associated to ferrite at 44.65°, and that to the left demonstrates that wustite appeared only on the ferritic sample.

On the oxidised samples, see Figure 7, the only peaks from the matrix that were identified are those of ferrite though their microstructure should be the same as for as-received and polished samples. The peak for ferrite at 44.65° (see the insert to the right in Figure 7) allowed

estimating the thickness of the oxide layer which appeared to be slightly thicker on the austempered alloy and thinner on the pearlitic one. These thicknesses were estimated of the order of 2 μm which is a bit smaller than what could be evaluated from Figure 5.

Table 3. Phases detected by X-rays. Only the oxides are reported for the oxidised samples for which only the ferrite peak of the matrix was identified.

| Sample | As-received | Polished | Oxidised |
|-------------|-------------|-----------|---|
| Ferritic | F + C | F | FeO + Fe ₂ O ₃ + Fe ₃ O ₄ |
| Pearlitic | F + C | F + C | Fe ₂ O ₃ + Fe ₃ O ₄ |
| Austempered | F | F + A + H | Fe ₂ O ₃ + Fe ₃ O ₄ |

Analysis of the X-rays records in Figure 7 allowed identifying only iron oxides on the oxidised samples. All three oxides, haematite Fe₂O₃ (rhombohedral, a = 5.04 Å, c = 13.75 Å), magnetite Fe₃O₄ (cubic, a = 8.39 Å) and wustite FeO (cubic, a = 4.29 Å), could be observed depending on the samples as listed in Table 3. Haematite and magnetite could be identified in all oxidised samples, while a small amount of wustite was only observed on the ferritic sample (see the insert to the left in Figure 7).

Conclusion

Decreasing initial surface roughness improves the adherence strength of the primer as measured with the pull-off test, and this improvement is enhanced after limited oxidation of the surface. On the contrary, increasing the amount of carbides in the microstructure decreases this strength, and this may well be related with the low polarity of carbides. After exposure to water, excellent adherence of the primer may be ensured by a limited pre-oxidation of the surface.

Acknowledgment

This work was prepared in the framework of the associated international laboratory "Functional Composite Materials (FOCOMAT)" between France and Vietnam.

Disclosure statement

No potential conflict of interest was reported by the authors.

References

- [1] Hessel JL, Tator KB. Cast iron organic coatings, ASM Handbook, Vol. 1A. Cast Iron Science and Technology; 2017. p. 338–354.
- [2] Corrosion of cast irons, ASM Handbook, Vol. 1A. Cast iron science and technology; 2017. p. 502–510.
- [3] Hemanth J. The solidification and corrosion behaviour of austempered chilled ductile iron. *J Mater Process Technol.* 2000;101:159–166.
- [4] Sosa AD, Echeverria MD, Moncada OJ, et al. Surface reactivity of thin wall ferritic ductile iron. The effect of nodule count and grinding variables. *Mater Lett.* 2008;62:100–102.
- [5] Sosa AD, Echeverria MD, Moncada OJ, et al. Surface reactivity of thin wall ferritic ductile iron. The effect of nodule count and microstructure. *NACE Corrosion;* 2008. paper #08252.
- [6] Sosa AD, Rosales CS, Boeri RE, et al. Corrosion mechanism in ADI parts. *Int J Cast Met Res.* 2016;29:105–110.
- [7] Medynski D, Janus A, Samociuk B, et al. Effect of microstructures on working properties of nickel-manganese-copper cast iron. *Metals.* 2018;8:341.
- [8] Ammar AU, Shadid M, Ahmed MK, et al. Electrochemical study of polymer and ceramic-based nanocomposite coatings for protection of cast iron pipeline. *Materials.* 2018;11:332.
- [9] Trinh AT, Nguyen TT, Thai TT, et al. Improvement of adherence and anticorrosion properties of an epoxy-polyamide coating on steel by incorporation of an indole-3 butyric acid-modified nanomagnetite. *J Coat Technol Res.* 2016;13:489–499.
- [10] Funke W. Problems and progress in organic coatings. *Prog Org Coat.* 1997;31:5–9.
- [11] Wielant J, Hauffman T, Blajiev O, et al. Influence of the iron oxide acid-base properties on the chemisorption of model epoxy compounds studied by XPS. *J Phys Chem C.* 2007;111:13177–13184.
- [12] <http://www.icdd.com/>
- [13] Dorazil E. High strength austempered ductile cast iron. Ellis Horwood Ltd; 1991.
- [14] Yang J, Putatunda SK. Influence of a novel two-step austempering process on the strain-hardening behaviour of austempered ductile cast iron (ADI). *Mater Sci Eng A.* 2004;382:265–279.